https://doi.org/10.5194/ar-2026-6
Preprint. Discussion started: 4 February 2026

Iberulite fall and formation mechanism during a Sahara dust event in Switzerland in February 2021

Bernard Grobety [1,3], Philippe Favreau [2], Juanita Rausch [1], David Jaramillo [1], Martin Steinbacher [4], Christoph Neururer [3]

[1] Particle Vision GmbH, Passage du Cardinal 13B, 1700 Fribourg, Switzerland; bernard.grobety@unifr.ch, juanita.rausch@particle-vision.ch, david.jaramillo@particle-vision.ch
[2] Service de l'air, du bruit et des rayonnements non ionisants (SABRA), Geneva Cantonal Office for the Environment, 1205 Geneva, Switzerland ; philippe.favreau@etat.ge.ch
[3] Geoscience Department, University of Fribourg, Chemin du Musée 6, 1700, Fribourg, Switzerland ; christoph.neururer@unifr.ch
[4] Empa, Laboratory for Air Pollution and Evironmental Technology, 8600 Duebendorf, Switzerland; Martin.Steinbacher@empa.ch

Correspondence to: Bernard Grobety (bernard.grobety@unifr.ch)

Abstract. Sahara dust events can promote the formation of micrometer-sized spherical mineral aggregates known as iberulites as they are usually found on the Iberian Peninsula. Iberulites have not, to our knowledge, been reported from Central Europe. Two formation mechanisms – in- and below scavenging – have been given. Strong iberulite fall (IFs) were observed in Western Switzerland in February 2021 when large amounts of dust were transported from the Moroccan-Algerian border towards Central Europe during a Saharan Dust Event (SDE). In contrast to the previous IFs observed on the Iberian Peninsula, this IF occurred under low-temperature conditions e.g. near the freezing point in the cloud and at the surface. The relative humidity in the first 1000 m below the clouds decreased from 70 to 40%. and the comparison between particle-size distribution (PSD) within the iberulites and the dust PSD in the free atmosphere revealed a Greenfield gap in the iberulites, e.g., a lack of particles in the range 0.1-0.3µm relative to the dust in the free atmosphere. The meteorological conditions, the microstructure of the iberulites, and the presence of a Greenfield gap point to below-cloud scavenging as the most likely formation mechanism. Further discoveries of iberulite in Swiss SDE samples suggest that the phenomenon is widespread and not only limited to regions close to the dust source.

https://doi.org/10.5194/ar-2026-6
Preprint. Discussion started: 4 February 2026

1 Introduction

Sahara Dust Events (SDEs) reach about 10-40 times per year the European Alps and significantly contribute to the aerosol load above the region, with strongest influence from February to June, and October to November (Coen et al., 2004; Collaud Coen et al., 2025; Mauro et al., 2019; Flentje et al., 2015). SDEs in February and March particularly increased since 2020 (Cuevas-Agulló et al., 2024). Aerosol concentrations during these events often exceed the European and Swiss air quality standards and the WHO PM10 air quality guidelines. There is evidence that desert dust affects human health, e.g., increases in cardiovascular mortality and respiratory morbidity, but the evidence remains inconsistent when considering the dust's geographical origin (Fussell and Kelly, 2021; Tobias et al., 2019). Dust also affects climate and ecosystems (Buseck and Pósfai, 1999; Parajuli et al., 2022). Although the importance of dust is recognized, dust mineralogical studies are scarce (Engelbrecht and Derbyshire, 2010).

A special form of dust aerosol particles are giant spherule-shaped aggregates between 50 and 200 µm in diameter. These "microspherulites" are called iberulites, in reference to their first observation in southern Spain (Díaz-Hernández and Párraga, 2008). Such iberulites were also reported from Mallorca (Spain) (Fiol et al., 2005) and from Tenerife (Spain) (Cuadros et al., 2015), but no observations have been reported from regions North of the Alps. Such aggregates are thought to form inside raindrops by the coalescence of smaller droplets in a cloud, thereby increasing the number of condensation nuclei in the latter, or by the capture of particles below a cloud by drops as they fall to the ground (Díaz-Hernández and Párraga, 2008). A major SDE hit Switzerland at the beginning of February 2021. Systematic SDE monitoring is conducted in Switzerland at the Jungfraujoch Sphinx observatory (inlet altitude 3585 m above sea level ASL (Vollmer et al., 2020)) since 2001 (Collaud Coen et al., 2025). Due to its elevation and the negligible local emissions, Jungfraujoch is a suitable location to investigate long-range transport processes (Herrmann et al., 2015). The event on February 6th was detected as one of the strongest SDEs since its systematic monitoring in 2001 (Collaud Coen et al., 2025). The dust reached the Alps on February 6th, 2021in the afternoon. At Jungfraujoch, a record PM10 concentration of more than 700 µg m^{-3} was measured (NABEL, BAFU/Empa). The IF analyzed here happened at lower altitudes in the village of Saint Légier (canton of Vaud, 46.471° N, 6.877°E), the city of Fribourg (canton of Fribourg, 46.717° N 7.083° E), and the city of Geneva (canton of Geneva, 46.033° N, 6.117° E), all in western Switzerland. Until now, two formation processes of iberulites have been proposed: in- and below-cloud scavenging. The goal of the present work is to explore the aggregation mechanism in greater detail, leveraging the well-documented meteorological conditions during the fall in our case.

https://doi.org/10.5194/ar-2026-6
Preprint. Discussion started: 4 February 2026

2 Methods

2.1 Collection sites

The fall of the Iberulites was observed on the early afternoon of February 6th in St. Légier, Fribourg, and Geneva (Switzerland). The city of Fribourg (500-700 m ASL)) is 50 km NNE of Lake Geneva on the Swiss plateau, and the village of St. Légier (576 m ASL) is on the central northern shore of the same lake. The geology of the surroundings of both sites is dominated by calcareous mountains (Jura, Préalpes) (Trümpy, 1980; Matzenauer, 2011). In St.Légier, the iberulites were picked up from the ground with tweezers, and in Fribourg, an aluminum foil was laid on the ground, from which samples were collected with a fine spatula. The iberulites were gently deposited onto two different substrates: head specimen mounts and boron substrates (see below).

The high-Alpine station Jungfraujoch (7.98° N, 46.55° E; 3580 m ASL), lies in the northern Swiss Alps. Its remote location, far from local anthropogenic sources, makes it ideally suited for monitoring background atmospheric conditions over central Europe. Jungfraujoch hosts a comprehensive long-term in-situ monitoring program for aerosols and trace gas as a contribution to the Global Atmosphere Watch (GAW) program of the World Meteorological Organization (WMO) (Bukowiecki et al., 2016) and is part of the Swiss National Air Pollution Monitoring Network (Hüglin, 2021).

2.1 Meteorological data

Meteorological data were obtained from radio sounding balloons, which are launched by the Federal Office for Meteorology and Climatology of Switzerland (MeteoSwiss) station in Payerne (46.817° N, 6.933° E), twice a day (23:00 and 11:00 h UTC). Payerne is located 17 km west and 47 km north of the collection sites in Fribourg and St. Légier, respectively. The station is equipped with a Raman lidar, ceilometers, and a Doppler radar to measure precipitation, aerosol concentration, and wind profiles. On February 6th, the ceilometer profile series from Payerne exhibited gaps in the morning and smaller ones in the afternoon due to ground fog. The area is also covered by two weather radars: one on La Dole Mountain (46.425°N, 6.099°E), west of St. Légier and near Geneva, and the other on the Plaine Morte (46.383°N, 7.500°E), in the central Bernese Alps southeast of the two collection sites.

The size distributions of fine-mode and coarse-mode aerosol at JFJ have been measured by a home-built Scanning Mobility Particle Size Spectrometer (SMPS) (Wiedensohler et al., 2012; Jurányi et al., 2011) and by a white-light optical particle size spectrometer (FIDAS, Palas GmbH, Germany) (Fischer and Hüglin, 2024), respectively.

The dust RGB product, based on three infrared channels of the Spinning Enhanced Visible and InfraRed Imager (SEVIRI) on EUMETSAT's MSG-11 satellite (https://www.eumetsat.int/0-degree-service), was used to determine the origin of the dust arriving in the afternoon over western Switzerland. The plume trajectory was traced on satellite images using the approach described by (Ashpole and Washington, 2013). The visually determined dust trajectories were verified by both forward and backward trajectory calculations using the Hybrid-Single Particle Lagrangian Integrated Trajectory (HYSPLIT) model

https://doi.org/10.5194/ar-2026-6
Preprint. Discussion started: 4 February 2026

developed by the National Oceanic and Atmospheric Administration's (NOAA) Air Resources Laboratory (ARL) (Draxler and Rolph, 2003). HYSPLIT uses archived 3-dimensional meteorological fields generated from ground and satellite observations, as well as short-term forecasts. For the present back-trajectory calculations, the Global Forecast System (GFS) dataset from the National Centers for Environmental Prediction (NCEP) at 0.25° resolution was used. The backward trajectories were calculated for an arrival time over Fribourg at an altitude of 2000 m above ground level (AGL) between 12:00 and 18:00 UTC on February 6th (approximately the level of the highest density of the arriving cloud). The forward calculations were done with a starting point in the center of the first dust plume observed in the satellite images.

The source meteorological data were extracted using the Real-time Environmental Applications and Display sYstem (READY) from the archived Global Data Assimilation System (GDAS) (Rolph et al., 2017). The data were obtained for the center of the primary dust source observed in the satellite image, e.g., 33.8°N, 1.5°W.

2.3 Scanning Electron (SEM) and Optical Polarization Microscopy (OPM) analyses

Single particles and iberulites were separated from bulk samples using an Olympus SZX12 binocular (Tokyo, Japan). They were transferred with a fine spatula and gently deposited onto a ½" pin stub mount (Ted Pella, Redding, CA, USA) previously coated with 12 mm Pelco tabs (Ted Pella, Redding, CA, USA) or onto homemade polished boron substrates. The latter were used to improve the contrast of low-atomic-number particles, such as soot (carbon). Each sample (area depending on particle load on the sample surface) was analyzed using automated SEM/EDX single-particle analysis (also known as Computer-Controlled SEM, CCSEM). For this purpose, a Zeiss Gemini 300 Field Emission Gun (FEG)-SEM equipped with an Oxford X-MAX EDS detector with an 80 mm^2 window, a high-efficiency four-quadrant Back Scattered Electron (BSE) detector, and the particle analysis software included in AZtecFeature (Oxford Instruments) at Particle Vision (Fribourg, Switzerland) was used. The analyses were performed at 20 kV. Particles deposited on the boron substrate were recognized by simple gray-value (i.e., BSE intensity) thresholding. EDX analyses were performed for each recognized particle. A "ZAF" correction (PAP version of the f(ρz) formalism (Pouchou and Pichoir, 1985) was applied automatically by the AZtec software to the raw data to calculate elemental concentrations. Quantification of the analyses was performed using factory-delivered standard measurements. The ZAF procedure is valid only for homogeneous samples with smooth surfaces perpendicular to the beam and considerably thicker than the excitation volume. Neither condition is met for the particles in our case. However, several authors (Weinbruch et al., 1997; Meier et al., 2018; Kandler et al., 2018) have shown that for particles larger than 1 µm in diameter, the relative standard deviation of corrected concentrations of major elements is approximately 2%. In contrast, for minor elements, the deviation is considerably larger (Kandler et al., 2018). As only particles with diameters > 1 µm were considered in the further processing of the data, the ZAF-corrected concentration values were retained without applying more sophisticated correction procedures. The standard deviation in ZAF-corrected concentrations measured in particles increases proportionally with the acceleration voltage (equivalent to increasing excitation volume). The measurement voltage (12 kV) is the lowest possible to excite characteristic X-ray lines for all elements present in the sample. Several blank analyses of empty boron substrates have shown that under the applied analytical conditions, the substrate surface contains only the element boron and that in an area of ca. 1 mm², a maximum of five particles were present on unexposed substrates. These particles are organic in nature and most likely follicles. Images obtained with both the optical microscope and the SEM were used to characterize the size distribution of the iberulites and their microstructure using Avizo software (Thermo Fisher).

The picked iberulites were placed in a round 1-inch container and filled with an impregnation resin. The resulting cylindrical samples were polished on the top side containing the iberulites and analyzed with a FEI Sirion FEG microscope (20 kV) equipped with the same EDS system as the Zeiss microscope above. A BSE image of the polished section was also segmented using Avizo software (Thermo Fisher), allowing the counting of individual particles and the determination of their equivalent spherical diameter, as well as the corresponding size distribution. Due to the resolution of the segmentation process, only particles larger than 0.05 µm are possible to be recognized and counted.

2.4 X-ray diffraction

A loose single dust particle sample, containing no iberulites but collected during the same period when the iberulites fell in Fribourg, was analyzed with a Rigaku Ultima IV diffractometer equipped with a Position Sensitive Detector (PSD). Diffractograms were recorded from 5° to 70° 2θ in step-scan mode (0.02°/step and 1 min/°). The copper X-ray tube was operated at 40 kV and 40 mA. The CuKα-radiation was filtered with a nickel foil. Quantitative phase analysis by Rietveld refinement (Bish and Post, 1993) was performed on the recorded patterns using the PDXL2 software package (Rigaku). The refined instrumental parameters are the zero shift, the sample displacement, and the peak shape, modelled using a Pseudo-Voigt profile. The structure parameters for the phases present in the sample were taken from the International Centre for Diffraction Data database, but only the scale factor, the unit-cell parameters, the isotropic overall temperature factor, and, in some cases, the preferred-orientation parameter (phyllosilicates, calcite) were refined using the March-Dollase (Dollase, 1986)formalism. The fractions of the phases present were determined through the scale factors. The atomic positions and site occupancies were held fixed during refinement. Iterations were performed until the refinement converged.

3 Results

3.1 Dust source and trajectory

The HYSPLIT backtrajectory calculations for air masses arriving over Fribourg in the early afternoon of February 6th originated in NW Africa (Fig. 1) between the southern Moroccan border and northwestern Algeria, a region. Satellite images showed the appearance of a dust plume (Fig. 2) in a region called "Haut Plateau". The air masses arriving during the afternoon and evening of February 5th over the Haut Plateau are at altitudes between 1000 m and 2000 m AGL, i.e., well within the Planetary Boundary Layer (PBL, Fig. 3). On February 5th, the upper limit of the PBL in the Haut Plateau region moved up to

https://doi.org/10.5194/ar-2026-6
Preprint. Discussion started: 4 February 2026

3500 m AGL, and the velocity in the surface air layer (10 m above ground) increased from 40 km/h to about 70 km/h. Weather stations in the Atlas Mountains recorded hurricane-force gusts (e.g., 117 km/h on 05.02.21 in Midelt, Morocco (Hoshyaripour, 2021). This is clearly above the threshold wind speed for dust emissions given for western Algeria (Marticorena et al., 1997).

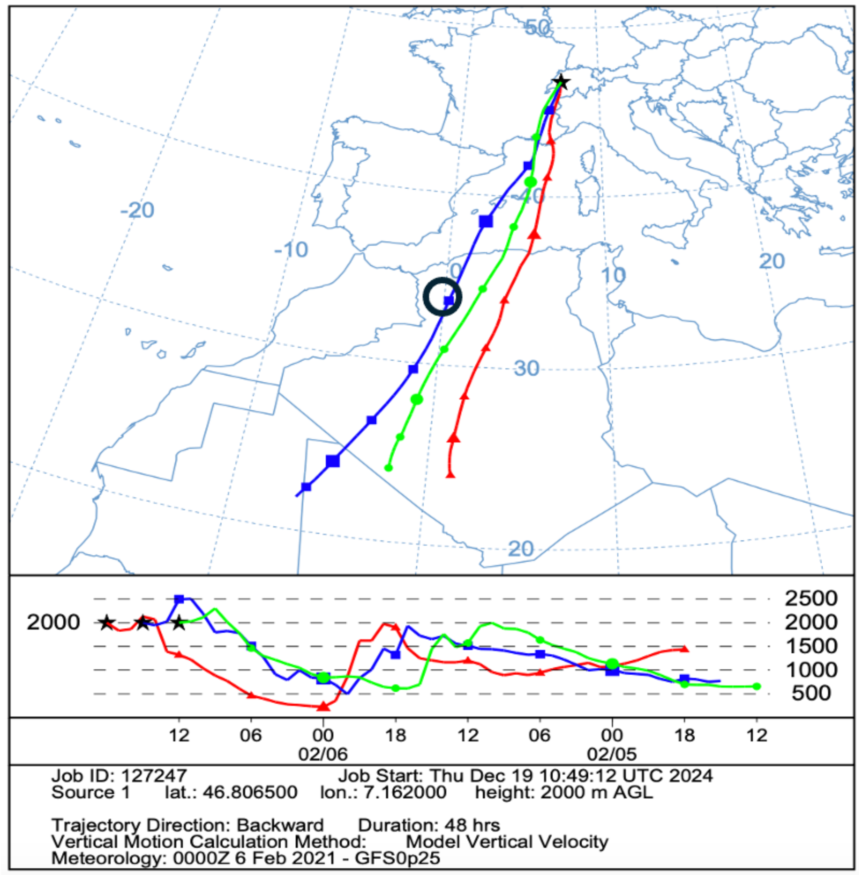

Figure 1: Back trajectories for air masses arriving over Payerne at an altitude of 2000m AGL during February 6th between 12:00 and 18:00 UTC. The black circle shows the location of the first appearance of the dust plume entrained across the Mediterranean Sea towards central Europe .

https://doi.org/10.5194/ar-2026-6
Preprint. Discussion started: 4 February 2026

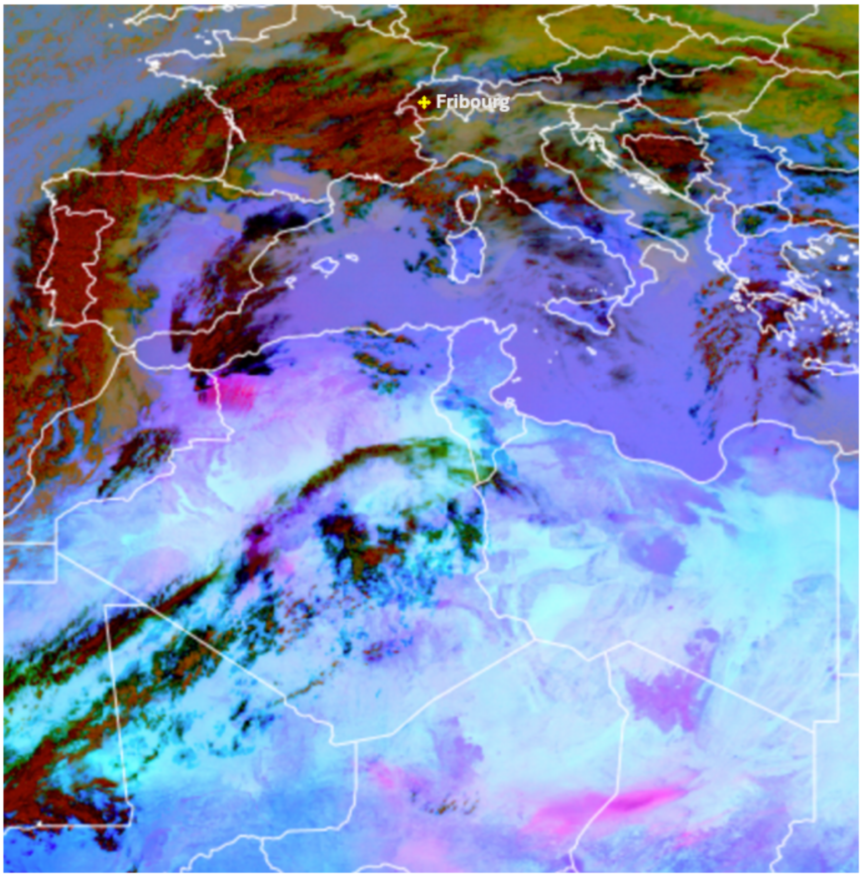

Figure 2: Satellite RGB image (5.2.2021. 22:00 UTC) from the SEVIRI dust product, showing the presence of dust by pink colors. The dust plume transported to Central Europe is seen east of the Moroccan – Algerian border.

https://doi.org/10.5194/ar-2026-6
Preprint. Discussion started: 4 February 2026

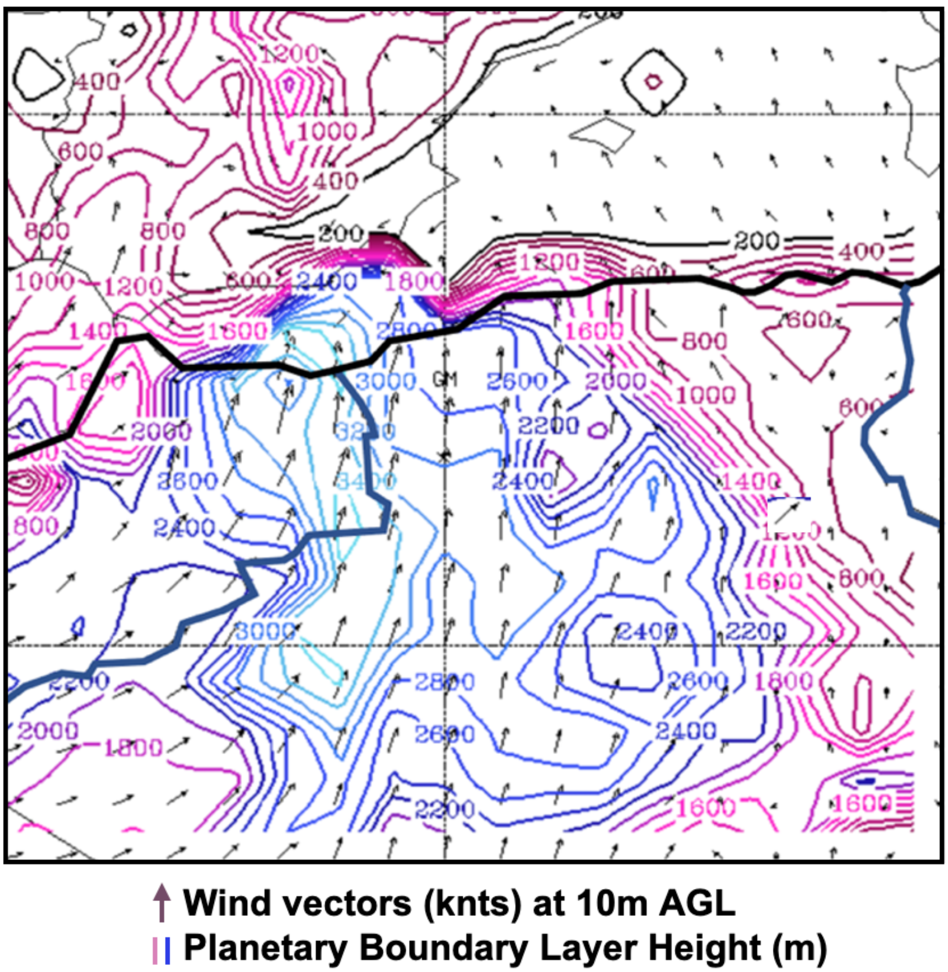

Figure 3: Map showing the upper boundary in meters AGL of the PBL over the Maghreb on February 5th at 12 h UTC. The arrows are wind vectors on the ground. The latter increases with increasing PBL depth (READY output (Rolph et al., 2017)).

The dust plume was entrained in a NE direction toward the Mediterranean Sea, where a low-pressure system formed. The associated warm conveyor belt lifted the dust to higher altitudes and transported it with the polar jet across the Mediterranean Sea toward the Alps, a process referred to as an "atmospheric river" (Francis et al., 2022; Rautela et al., 2024). Source sensitivities were calculated for Saharan dust (fine mode) arriving at JFJ using FLEXPART to obtain the backward trajectories and to detect general surface contact of air masses over the Saharan desert (Collaud Coen et al., 2025). The calculated sensitivities indicate that the direct pathway from the Sahara over the Mediterranean to the Alps is the most frequent.

3.2 Local meteorology

Ground temperature measurements and the emagram from the radio sonde released at 11:00 UTC in Payerne revealed relatively high temperatures for February 6th in Western Switzerland (8° C at the ground and a zero-degree level at 2500 m ASL) and a

https://doi.org/10.5194/ar-2026-6
Preprint. Discussion started: 4 February 2026

typical inversion situation (Fig. 4a). In contrast to conditions during previous IFs over the Iberian Peninsula (Diaz-Hernandez and Sanchez-Navas, 2016) the temperature was much lower. The vertical profile of relative humidity (RH) was complex. RH decreased from 100 % at the ground level to a very low 40 % at 1000 m, then increased to 85 % at 3500 m ASL (Fig. 4b).

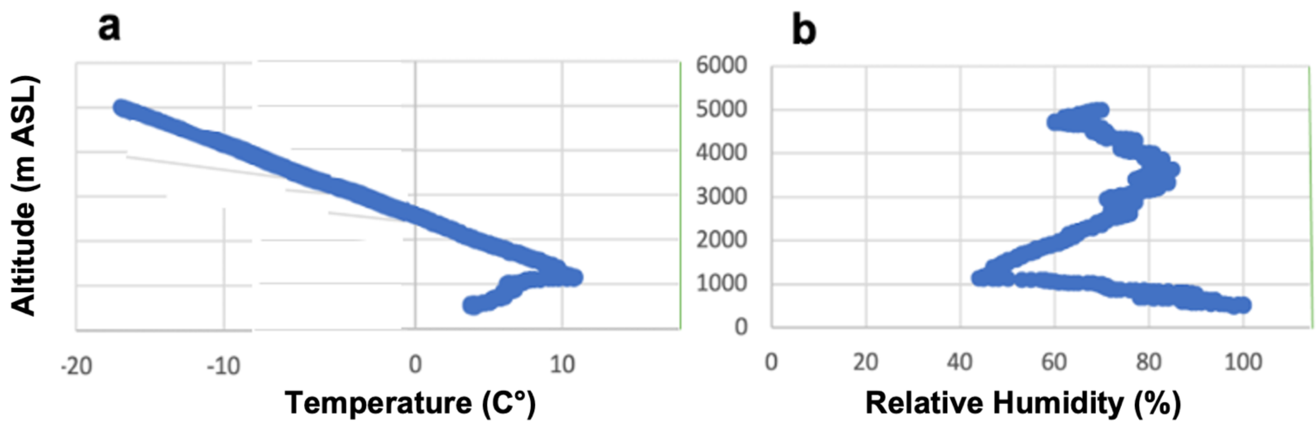

Figure 4: Temperature (a) and relative humidity (b) as a function of altitude from the radio sounding. The sounding balloon was released in Payerne at 11:00 h UTC (MeteoSwiss).

The Payerne ceilometer time profile (Fig. 5) shows a cloud base at 5000 m ASL at midnight, with reflections that may be due to aerosol (SDE) or ice particles, extending from the cloud base down to 3500 m. Early in the morning, the cloud base lowered to 4000 m, and the reflections extended down to 2500 m. The below-cloud reflections have a streaky appearance in the ceilogram. After a large gap in ceilometer recordings between 9:00 and 11:00 h UTC, a reflection wall extending from 3500 m to the ground appeared. These strong reflections from dust particles persisted throughout the day. The cloud base lowered from 4000 m to 2000 m during the evening. At around 22:30 h, three short periods with very strong reflections were observed; during those times, precipitation was recorded on the ground. After 23:00 h, the reflections became less intense.

https://doi.org/10.5194/ar-2026-6
Preprint. Discussion started: 4 February 2026

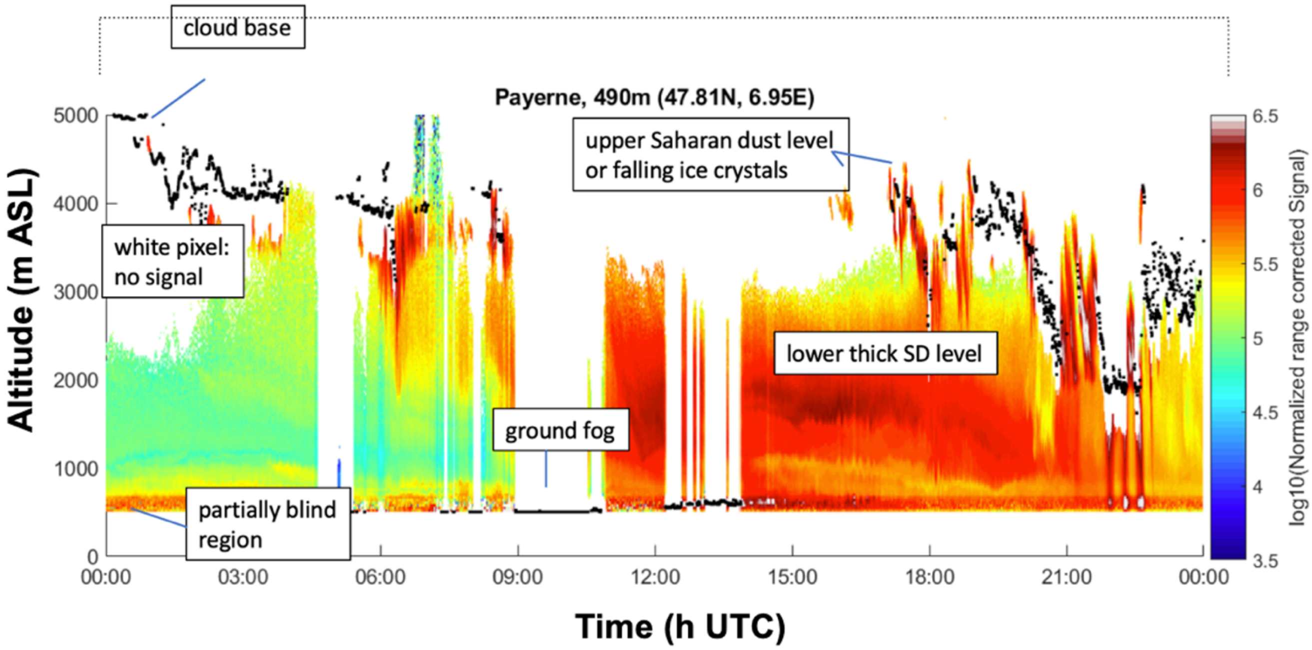

Figure 5: Ceilogram profile for February 6th (MeteoSwiss)

Lidar measurements were used to derive a mass-concentration profile (Fig. 6) across the dust cloud, with the altitude range between 4000 and 5000 m serving as the "no aerosol" reference. The profile was derived using a lidar ratio of 0.57 $m^2/sr \pm 9$ sr at 532 nm (Haarig et al., 2022), an Ångström coefficient of 0.5 for long-range transported dust in northern European regions (Ansmann et al., 2001), and a mass extinction ratio at 532 nm of 0.47 ± 0.04 m^2 g^{-1} (Nemuc et al., 2013). The profile exhibited three peaks. The maximum concentration of 81 µg m^{-3} was observed at an altitude of 1675 m. The second-largest concentration was recorded just above the ground, and a third small peak was located just above the cloud base at approximately 3500 m.

https://doi.org/10.5194/ar-2026-6
Preprint. Discussion started: 4 February 2026

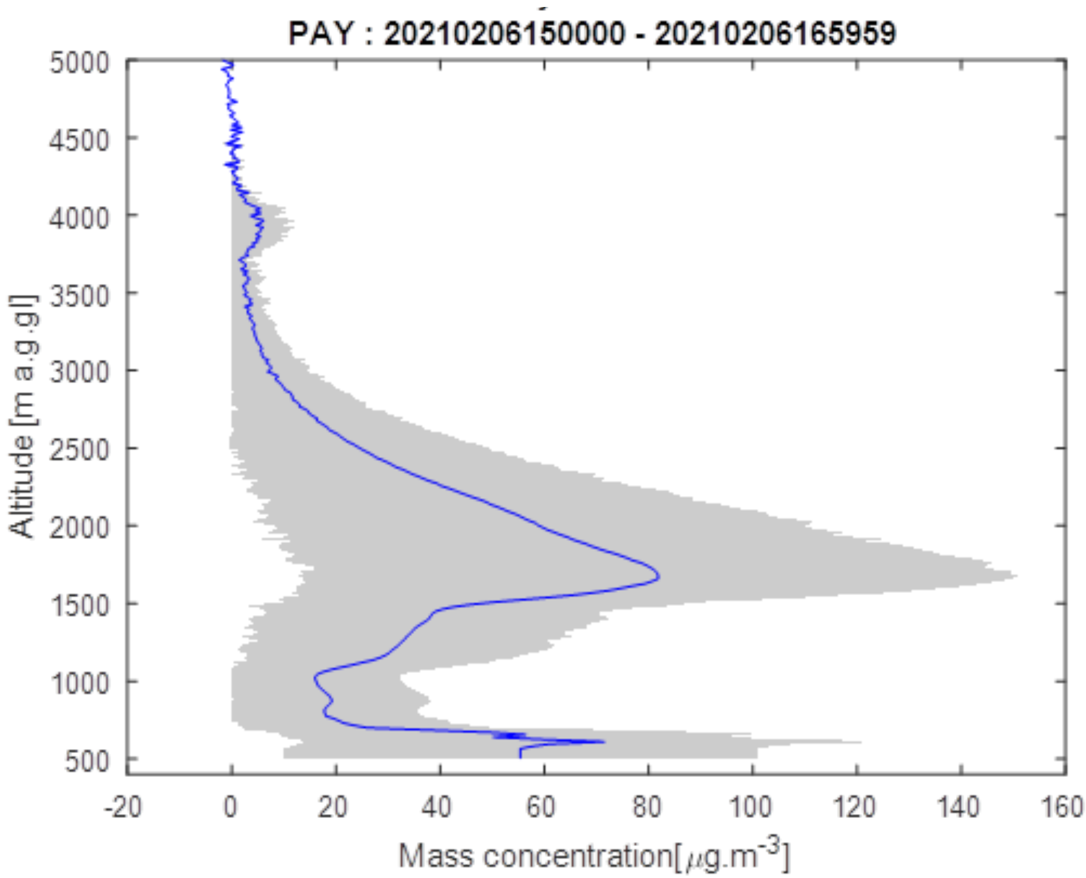

Figure 6: Aerosol mass concentration profile across the dust cloud (MeteoSwiss).

3.3 Iberulites collected in Fribourg and St. Légier

In Fribourg, very large particles with diameters exceeding 30 µm were detected. Unusual giant single particles have been observed previously following long-range transport of Saharan dust (Van Der Does et al., 2018). Rapid transport, high turbulence, and electrical forces are thought to compensate for the particles' weight**.** In our case, the large "particles" were not single particles but multimineral particle aggregates with spherical to slightly ellipsoidal shapes, known as iberulites after their first recording on the Iberian Peninsula (Fig. 7) (Díaz-Hernández and Párraga, 2008). The cores of the iberulites are composed mainly of coarser mineral grains (Fig. 8 e,f, and Fig. 9) that have accreted without a visible cement matrix. Except for a thin, dense surface layer, the iberulite cores show no internal structure, such as layering or preferential grain orientation. The iberulites collected in St Légier (n = 425) are larger than the Iberian specimens, with a mean diameter of 113 µm (range: 43 – 365 µm).

https://doi.org/10.5194/ar-2026-6
Preprint. Discussion started: 4 February 2026

Figure 7: Light microscopy image of iberulites collected in St Légier.

https://doi.org/10.5194/ar-2026-6
Preprint. Discussion started: 4 February 2026

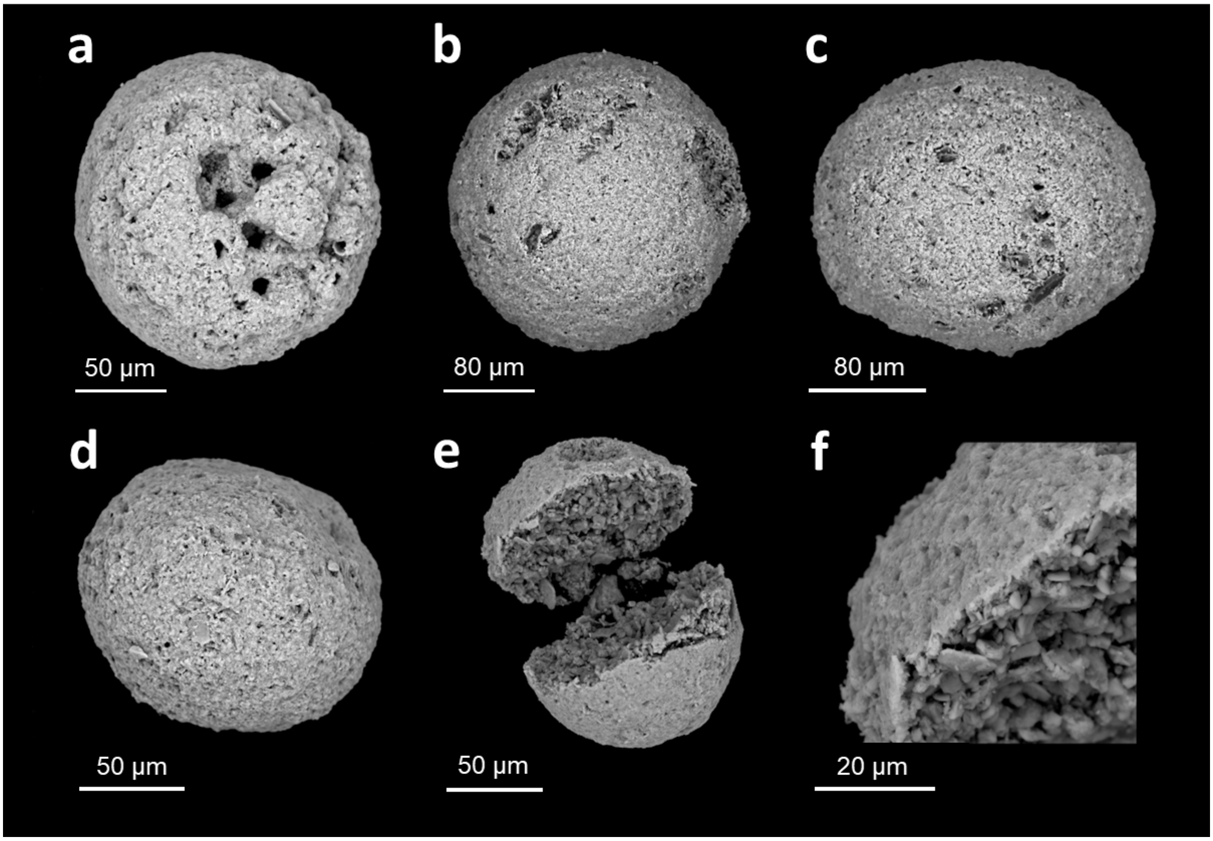

Figure 8: SEM images of some iberulites collected in St Légier on February 6th, 2021. Figure 8 f shows the fine-grained rim of an iberulite.

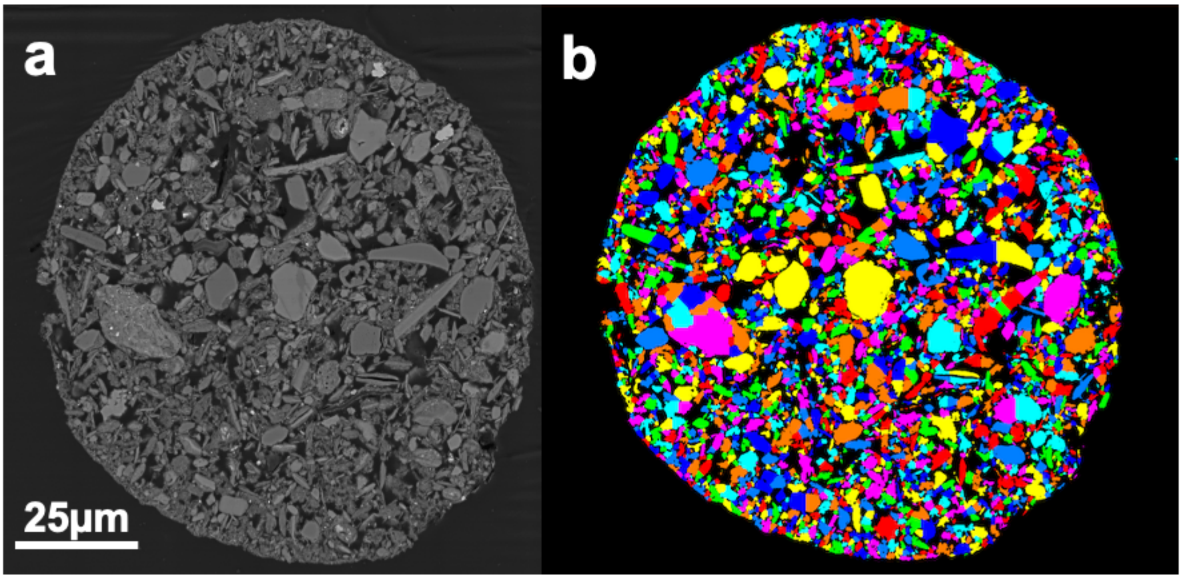

Figure 9: (a) BSE image of a polished section through an iberulite, and (b) the corresponding segmentation obtained from AVIZO.

Most iberulites have smooth surfaces with few large surface pores (Fig. 8), most likely due to particles that have been ejected from the aggregates. Spherical surface depressions, e.g., vortices formed by the flow of air around the aggregates (Díaz-Hernández and Párraga, 2008), are rare.

3.4 PSDs at JFJ and inside the iberulites

The long-term PSD measured with SMPS and CPC at JFJ, when the latter was in the cloud, was taken as representative of the PSD in the main dust layer. During times when JFJ is cloud-free, above the PBL, and no Saharan dust present the PSD has two modes: a stronger one near 0.05 µm and a weaker one between 0.15 and 0.4 µm (Nessler et al., 2003; Herrmann et al., 2015; Bukowiecki et al., 2016). The PSD measured at 11:00 UTC on February 6th during the SDE is monomodal, with a maximum near 0.150 µm (see Fig. 10, yellow bars), and shows much higher concentrations than measurements without SDEs, similar to PSDs observed in previous Saharan dust episodes at JFJ (Chou et al., 2011). Coarse-mode particles arriving at JFJ were well documented in previous particle volume distributions, with a mode at 1.4 µm (Schwikowski et al., 1995).
Saharan dust clouds transported over long distances, such as to Barbados during the SALTRACE campaign (Weinzierl et al., 2017), to Aeronet sites in the eastern Caribbean (Velasco-Merino et al., 2018), over the Mediterranean Sea during the ChArMEx/ADRIMED campaign (Denjean et al., 2016), and over Cape Verde during the SAMUN2 campaign (Weinzierl et al., 2011) have similar PSDs. The largest particles observed at the Caribbean sites are well above the maximum diameter expected for settling due to Stokes' law during transport. The modes observed at JFJ and in the campaigns cited above are

similar to the PSDs observed in the source regions (Panta et al., 2023; Bencherif et al., 2022; Dubovik et al., 2006), but are lower in concentration and lack particles > 30µm.

The equivalent volume diameter d_{ve} and the shape factor χ of the particles inside the iberulites were estimated following (Ott and Peters, 2008):

$$d_{ve} = \sqrt{\frac{4A}{\pi}} \quad (1)$$

$$\chi = \frac{p^2}{4\pi A} = \frac{1}{cicularity} \quad (2)$$

with A the area covered by and p the perimeter of the particles in the segmented BSE image. The PSDs inside the iberulites are ± monomodal with a maximum at 2.5µm (Fig. 10, blue bars), i.e., much larger than the value for the Saharan dust sampled in JFJ, i.e., 0.15µm (Fig. 10, yellow bars). The PSD of the particles inside the iberulites shows a minimum where the JFJ has a maximum. The average aspect ratio (AR) compares to the median AR of long-range transported Saharan dust particles measured in the Caribbean during the PRIDE experiment over Puerto Rico (1.93 vs 1.9) (Reid et al., 2003), but is larger than the value obtained for short- to medium-range transported Saharan dust over Tenerife (1.64) (Kandler et al., 2007) and during the AMMA SOP0/DABEX campaign, e.g., samples collected on site and during flights over the western Sahara (1.7) (Chou et al., 2008). This increase in particle asphericity during transport is likely due to the preferential settling of spherical particles, which have a greater terminal fall speed than aspherical particles of the same volume (Mallios et al., 2020). In the present case AR ranges from 1.0 to 6.0 and, as previously reported (Huang et al., 2020), shows little dependence on dust size.

In order to compare the SMPS with the SEM derived PSDs, d_m of the first has to be converted to volume equivalent diameter d_{ve} (Decarlo et al., 2004):

$$d_{ve} = \frac{d_m C_c(d_m)}{C_c(d_{ve})\chi} = CF d_m \quad (3)$$

with $C_c(d_m)/C_c(d_{ve})$, the Cunningham slip correction factor ratio between the mobility and volume equivalent diameters, the dynamic shape factor χ, and the conversion factor CF. $C_c(d_{ve})$ is unknown. The ratio $C_c(d_m)/C_c(d_{ve})$ (the ratio given by Peng et al. is the reverse of the latter one!) has been measured only(?) for salt particles smaller than 600 nm. It is always less than one, increases with size, and decreases with aspect ratio (Peng and Liu, 2022). In contrast to the aspect ratios, shape factors appear to depend strongly on size. They are size-, flow-regime (Alexander et al., 2016), and orientation (Cheng et al., 1988) dependent, ranging from near unity for smaller particles to a median value of 3 for the largest particles. The average χ of the particles inside the iberulites is 1.46, very close to 1.4 reported for most dust particles in the 2 to 10 µm range (Kaaden et al., 2009). Overall, CF is mostly smaller than 1. The converted volume-equivalent diameters are smaller than the mobility diameters, and

https://doi.org/10.5194/ar-2026-6
Preprint. Discussion started: 4 February 2026

the PSD shifts to the left. For a particle with a diameter of 0.2 or 2.0 µm, both with an axis ratio of 1.93, and corresponding values of $C_c(d_m)/C_c(d_{ve})$ and χ, the shift is 1 bin to the left for both, e.g., the maximum of the JFJ PSD is shifted from the (0.16 – 0.32µm) to the (0.16 – 0.32µm) bin. Overall, d_{ve} is always smaller than d_m.

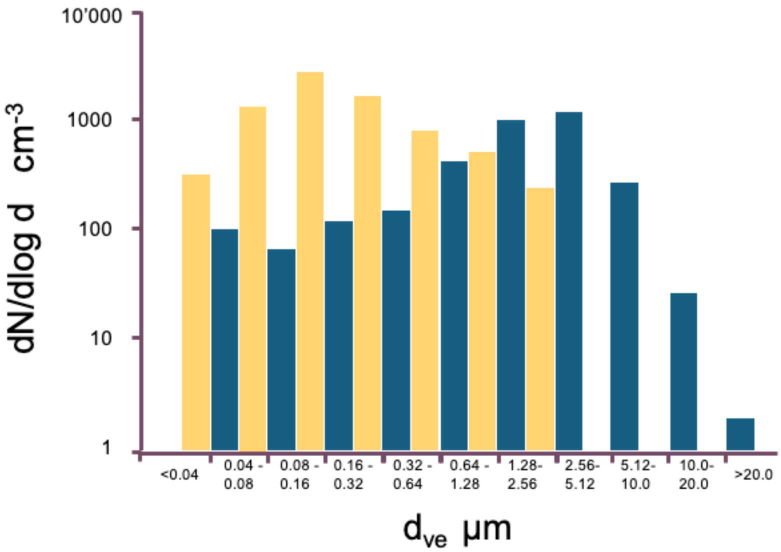

Figure 10: Yellow bars: Jungfraujoch PSD measured February 6th at 12:00 (shifted 1bin to the left relative to the original data, s. text), blue bars: particle size distribution measured for an iberulite sample collected in St. Légier.

3.5 Composition of Saharan dust and iberulites

3.5.1 XRD -results (Rietveld analysis) and single particle analyses

X-ray diffraction (Fig. 11) showed that iberulites contain phyllosilicates (illite, muscovite, and kaolinite, totaling 34.1 wt%), followed by carbonates (27.0 wt% calcite, 4.0 wt% dolomite) and quartz (23.3 wt%). The concentrations of gypsum and halite were below the detection limit.

https://doi.org/10.5194/ar-2026-6
Preprint. Discussion started: 4 February 2026

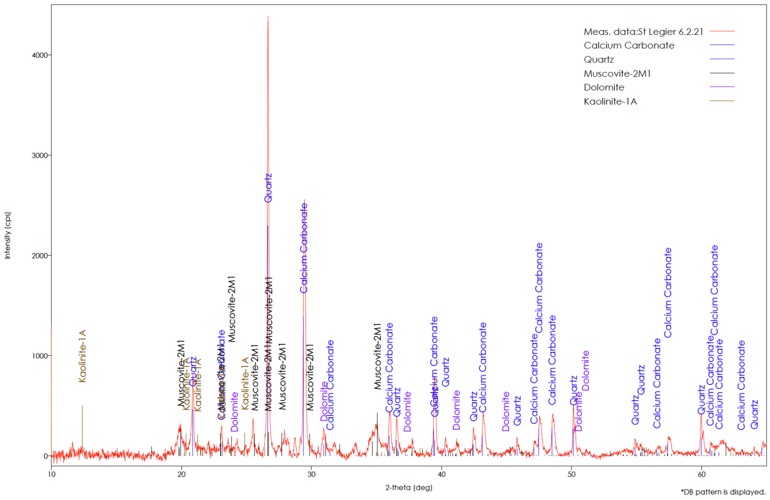

Figure 11 X-ray diffraction pattern of the St. Légier sample.

3.5.2 EDS analysis

Analysis of individual particles within an iberulite confirms the XRD results. EDS analyses on the polished iberulite section have a resolution of 1 – 2 µm, depending on the thickness of the section and the local composition. Trends from the ideal muscovite composition toward the calcite composition, as well as toward the quartz compositions, in the (Mg+Fe+Si+K–Al–Ca) ternary diagram indicate that the analyses are mixtures of the three phases (Fig. 12 a). The ternary diagram (Mg+Fe+Si+K–S–Ca), with Mg+Fe+Si+K as the "silicate" corner and Ca as the "calcite" corner (Fig. 12 b), shows measurements mainly along the joint between the silicate and calcite corners, indicating mixed analyses between these corners, with some measurements scattered in the triangle silicates-calcite-gypsum, indicating mixed analyses among these phases or the presence of sulfur on other particle surfaces. A short trend from the silicate corner in the diagram (Mg+Fe+Si+K–Na-Cl) (Fig. 12 c) toward the halite composition indicates mixed analyses between these phases.

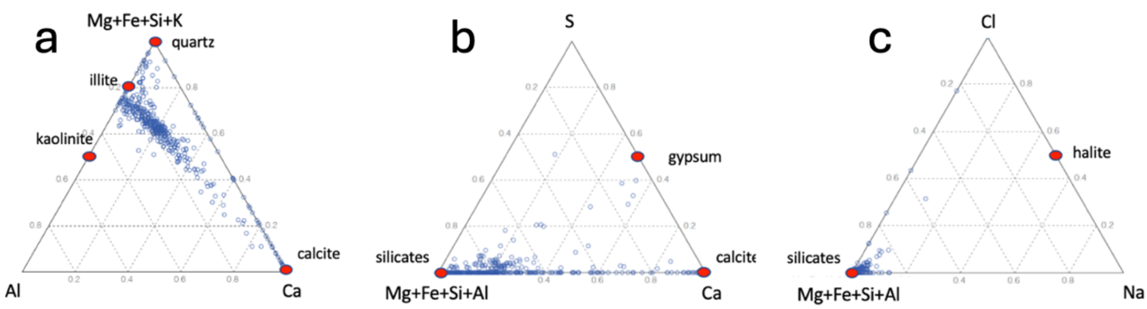

Figure 12: Ternary diagrams : (a) (Mg+Fe+Si+K–Al–Ca), (b) (Mg+Fe+Si+K–S–Ca), (c) (Mg+Fe+Si+K–S–Ca).

4. Discussion

https://doi.org/10.5194/ar-2026-6
Preprint. Discussion started: 4 February 2026

4.1 Dust composition

Dust from potential source areas (PSA) has been characterized by bulk chemistry (Kandler et al., 2007) and mineralogy (Scheuvens et al., 2013). Mineralogical fingerprints include phyllosilicates, such as the ratio of illite to kaolinite concentrations (I/K) (Caquineau et al., 1998; Chester and Johnson, 1971; Scheuvens et al., 2013). The general trends are increases in I/K from S to N and from E to W. The value for the present samples is approximately 2.9, consistent with values reported from the Western Sahara, e.g., >2 in NW Algeria and Morocco. High carbonate contents (>10 wt.%, calcite > dolomite) are also a fingerprint of dust from the northwestern part of Africa (Avila et al., 1997). Similar to illite, carbonate content decreases continuously toward the south (Paquet, 1984). The high carbonate content of dust emitted from the northern regions within and adjacent to the Atlas Mountains reflects the geology of those regions (Grousset et al., 1992).

4.2 Iberulite formation and internal structure

The IF on February 6th in Fribourg was observed in person. The meteorological conditions during the fall are therefore well known. Two mechanisms have been proposed for aggregating a large number of dust particles within a drop (Diaz-Hernandez and Sanchez-Navas, 2016; Párraga et al., 2021): 1. The coalescence of drops within a cloud increases the number of condensation nuclei within a single growing drop, i.e., in-cloud scavenging (ICS) (also denoted as 'nucleation scavenging'), or 2. the concentration increases through collisions between the particles and a drop below the cloud along its trajectory to the ground. This mechanism is called below-cloud scavenging (BCS) (also denoted as impaction scavenging) (Pruppacher and Klett, 2010). The BCS rate strongly depends on rainfall intensity, raindrop size distribution, and the drop's ability to collect particles, called the collection efficiency (CE) (Volken and Schumann, 1993; Slinn, 1977; Laakso et al., 2003).
CE is the number (or mass) of particles captured by a drop of a given size relative to the particle number in the cylindrical volume swept by the drop per unit trajectory length. If CE were independent of the properties of the drop, the particle, environmental parameters, and the capture processes, the grain-size distribution in the iberulite would reflect the size distribution of the dust in the volume traversed by the drop. However, this is not the case (see Fig. 10). The mechanisms contributing to the capture process depend on particle size and the fluid flow around the falling droplet.
If the drop with a radius *R* falls vertically, e.g., no deviation by wind, the maximum number of possible collisions *N* along a trajectory *l* within the dust layer with mass density M_d and particle density *d* can be calculated:

$$N = \frac{M_d * 2\pi R^2 * l}{\frac{4}{3}\pi r^3 \cdot d} \quad (4)$$

For particles >1µm in diameter colliding head- on with a droplet, bouncing is unlikely, and the sticking efficiency is taken as 100% (Pruppacher and Klett, 2010). However, for particles with radii between 0. 3 µm and 1µm, the CE, defined as the ratio of the total number of collisions given by eq. 4 to the number of particles captured by the droplet, is < 1. This is due to the airflow around the falling droplet. Particles within this size range, despite being on collision trajectories, follow the flow lines and are carried around the droplet. Larger particles, due to their inertia, cross the flow lines and impact the droplet, resulting in CE = 1 (capture by impaction). Small particles (< 0. 1 µm) that follow the flow lines may be pushed by Brownian motion into the droplet' s wake and deposited on its rear end (Brownian capture), and CE is also close to 1. Capture may also be due to thermophoretic and diffusiophoretic forces. Thermophoretic forces "push" aerosol particles toward a frozen drop during evaporation and away from it during vapor deposition. During diffusive crystal growth, a flow known as Stefan' s flow exists near the hydrometeor surface, exerting a force on nearby aerosol particles that pulls them toward the surface (Santachiara et al., 2023). Particles, independent of size, may follow the flow lines, but at some point the flow lines are closer to the drop's surface than the particle's radius; e.g., the particle meets the drop's surface and sticks to it (capture by interception). This process has a rather low capture efficiency. For particles with radii between 0.3 and 1.0 µm, none of the above- described capture processes is effective, and CE decreases by two orders of magnitude. This decrease in CE was first described by Greenfield (Greenfield, 1957), and the lack of particles in the 0.3 – 1,0 µm range is, therefore, referred to as the Greenfield gap. Comparing the PSD of the free aerosol - we took the JSF PSD as representative for the distribution for the PSD inside the Saharan dust cloud - and the one inside the iberulite, a shift of the maximum to larger sizes in the PSD inside the iberulite is apparent, e. g., the presence of a Greenfield gap in the expected range (see Fig. 10).

Although no precipitation was observed on the ground during the afternoon of February 6th, 2021, some iberulites striking car windshields were still wet, indicating that rainfall was present along the trajectory but had largely evaporated before reaching the ground. The dust concentration distribution from the ceilogram taken on the day of the iberulite fall in Payerne shows three maxima between 4500 m altitude and the ground. The dust concentration maxima within the cloud and just above the ground are less significant than the massive layer between 3000 m and 1000 m AGL.

The temperature at the upper boundary of the dust layer was below 0° C and turned positive around 2500 m. However, melting of the frozen hydrometeors most likely began at a much lower level due to the low relative humidity, in which the water vapor density of the surrounding air is lower than the equilibrium water vapor density of frozen hydrometeors at the freezing point; therefore, sublimation of water vapor occurs from the surface of the latter. Because of this sublimation process, latent cooling can push the surface temperature of the hydrometeor below 0 °C (Matsuo and Sasyo, 1981; Heymsfield et al., 2015). The width of the non-melting layer in the atmosphere increases nearly linearly with decreasing relative humidity, from 120 m at 90% to 700 m at 50%. The relative humidity at the top level of the main Sahara dust layer is around 70% and decreases with decreasing altitude. It is therefore probable that the melting level is displaced far into the massive Saharan dust layer.

Although difficult to distinguish from aerosol particles, the reflections just below the cloud base may originate from frozen hydrometeors. Both solid ice crystals and liquid drops can capture particles. Frozen hydrometeors can occur as small particles, columnar or planar crystals (branched = snowflakes), combinations of these, aggregates, and graupel, all with varying degrees of riming (Magono and Lee, 1966; Grazioli et al., 2015; Praz et al., 2017). Scavenging of aerosol particles by frozen hydrometeors is more complex than by raindrops because of their non-spherical shapes and falling behavior. With increasing Reynolds number and shape irregularity, the falling motion of frozen particles transitions from steady to periodically changing

https://doi.org/10.5194/ar-2026-6
Preprint. Discussion started: 4 February 2026

(fluttering, spiraling, zigzagging) and chaotic trajectories (Hashino et al., 2016; Kajikawa, 1992; Tagliavini et al., 2021; Mccorquodale and Westbrook, 2021; Stringham et al., 1969). Columnar ice particles align their long axis perpendicular to the (vertical) fall direction. Hexagonal ice plates and irregular snowflakes adopt a broadside orientation relative to the flow direction. Flow around such frozen hydrometeors is characterized by a deviating pattern around the front (Martin et al., 1980) and by eddies in the rear of the falling hydrometeor (Hashino et al., 2016; Wang et al., 2021). The distribution of dust particles (diameter 0.2 – 2.0 µm) on hexagonal ice plates shows increased concentration along the edges and corners (Prodi, 1976), whereas particles on snowflakes are distributed inhomogeneously (Ma et al., 2013).

Several studies on BSC (Feng, 2009; Kyrö et al., 2009; Paramonov et al., 2011) indicate that frozen hydrometeors are more effective scavengers of aerosol particles than rain on an equivalent water-content basis. The fluttering, zigzagging fall style of frozen hydrometeors prolongs their trajectories, thereby increasing the probability of collisions with aerosol particles and, consequently, CE. CE also increases with temperature and relative humidity. The highest CE has been recorded for mixed precipitation types and frozen hydrometeors at temperatures slightly above 0 °C. At these temperatures, frozen hydrometeors develop a stickier liquid layer at the surface. The increase in CE at higher RH is attributable to increased collector capacitance (Paramonov et al., 2011). The nature and size distribution of frozen hydrometeors also influence CE (Jung et al., 2015). CE decreases with increasing snowflake diameter, whereas dendrites and columns do not show this decreasing tendency. The largest CE was observed for columnar ice particles. The Greenfield gap in snowfall situations was in a smaller size range of 0.09-0.3 µm compared to the gap observed for rain. This range is also observed for the iberulites collected in the present fieldwork, supporting frozen hydrometeors as dust scavengers. The increased CE of frozen hydrometeors is probably also the reason for the larger diameters observed in Swiss iberulites compared to Iberian iberulites.

When frozen hydrometeors exit the non-melting zone, for example, by crossing the melting level, they melt or evaporate. They exhibit a wide range of melting behaviors (Oraltay and Hallett, 2005). Ice crystals melt from the outside inward and are covered with a water film. Columnar ice particles melt uniformly, forming a thin liquid film that, as melting continues, bunches into one or several liquid bulges along the column (Knight, 1979; Fujiyoshi, 1986). Further melting within the bulges is slower, and the bulges coalesce into a single spherical drop containing the remaining ice particles. In melting snowflakes, liquid droplets gather preferentially in concave regions at the intersection of dendrites. When the concave areas are filled, the meltwater flows out, forming a spherical drop around the leftover ice particles (Oraltay and Hallett, 2005; Leinonen and Lerber, 2018). In experiments using a levitation test rig to study the melting process, a single ice crystal became spherical at 68.6% of melting, independent of its initial shape (Yan and Palacios, 2024).

Field observations (Heymsfield et al., 2015) spanned the smallest to the largest particles. In contrast to earlier studies (Ohtake, 1969; Barthazy et al., 1998), the largest particle size increased through the melting layer due to aggregation (Mcfarquhar et al., 2007), because the particles become stickier due to the liquid layer covering their surfaces. The particle concentration did not increase, suggesting that particle breakup during the melting process is not significant. The behavior of scavenged aerosol particles within melting hydrometeors has not been reported to date. Most likely, they are included in the newly formed raindrop.

https://doi.org/10.5194/ar-2026-6
Preprint. Discussion started: 4 February 2026

Within and below the melting layer, due to the very low relative humidity (45% at 1000 m, at the bottom of the massive dust layer), raindrops will dry very rapidly. A technological analogue of this process is the (spray) drying of a powder suspension, which is used, e.g., in the ceramic, food, or pharmaceutical industry (Santos et al., 2018). The difference between the drying of a droplet in a spray drier and that of a rain droplet falling out of a cloud is the temperature difference between the droplet and the drying air stream, which is around 200°C in a spray drier. Droplets in a spray dryer relax into spherical shapes and are analogous to raindrops.

The latent heat of water evaporation induces a strong heat flux from the droplet surface into the gas stream. This, in turn, drives thermophoretic particle displacement toward the droplet surface and a specific microcirculation within a layer near the surface, driven by the surface tension gradient (Iskandar et al., 2003). This microcirculation entrains particles toward the droplet surface, leading to size- and density-based segregation. Smaller and/or less dense particles move faster toward the droplet surface, forming a thick surface layer. Coarser particles are concentrated in the core. Such a shell-core structure was observed in the present iberulite and has also been reported in the Iberian examples (Díaz-Hernández and Párraga, 2008; Párraga et al., 2021), with fine-grained phyllosilicates concentrated in the shell and coarse-grained quartz grains in the core.

5. Conclusion

To our knowledge, this analysis represents the first detailed study of iberulite fall in Switzerland. In contrast to the Iberian cases, the IF fall occurred under much colder conditions, e.g., temperatures around 0° and decreasing relative humidity along the fall trajectory. Iberulites form through the accumulation of particles inside raindrops. A comparison of the PSD inside the iberulites with the PSD measured in the dust cloud at the Jungfraujoch, which encountered the same cloud, revealed a Greenfield gap in the iberulite PSD, i.e., a lack of particles in the range between 0.1 and 0.3 µm. The presence of a Greenfield gap within the iberulites supports below-cloud scavenging, i.e., particle capture through collisions of particles with droplets below a cloud, as the mechanism for particle accumulation. The gap arises from particle trajectories in the flow around the falling droplet, which depend on particle size. The freezing temperature, low relative humidity, and ceilogram signals suggest that particle collisions occurred not with raindrops but with snowflakes or ice crystals. The latter are known to be better scavengers than raindrops.

Since 2021, more iberulites have been found in filter samples collected during SDEs in Switzerland. They will be analysed to confirm the findings and to gain a better understanding of the relationship between iberulite formation and meteorological conditions.

https://doi.org/10.5194/ar-2026-6
Preprint. Discussion started: 4 February 2026

Author contributions

BG designed the study. CN, BG, and JR performed the measurements. BG analyzed the data. MS provided data from Jungfraujoch. BG, JR, and DJ wrote the paper. All co-authors proofread and commented on the paper.

Competing interests

The authors declare that they have no conflict of interest..

Acknowledgements

The authors acknowledge Maxime Hervo from Meteoswiss for the supply of meteorological and lidar data. We thank also Mario Wannier for supplying iberulites collected in St. Légier. NOAA for HYSPLIT? SEVIRI? Originator of Figure 2? PSI for SMPS data from JFJ.

Financial support

This research received no external funding.

References

Alexander, J. M., Bell, D. M., Imre, D., Kleiber, P. D., Grassian, V. H., and Zelenyuk, A.: Measurement of size-dependent dynamic shape factors of quartz particles in two flow regimes, Aerosol Science and Technology, 50, 870–879, 10.1080/02786826.2016.1200006, 2016.

Ansmann, A., Bösenberg, J., Chaikovsky, A., Comerón, A., Eckhardt, S., Eixmann, R., Freudenthaler, V., Ginoux, P., Komguem, L., Linnè, H., Linné, H., Márquez, M. A. N. L., Matthias, V., Mattis, I., Mitev, V., Müller, D., Music, S., Nickovic, S., Pelon, J., Sauvage, L., Sobolewsky, P., Srivastava, M. K., Stohl, A., Torres, O., Vaughan, G., Wandinger, U., and Wiegner, M.: Longr range transport of Saharan dust to northern Europe: The 11th October 2001 outbreak observed with EARLINET, Journal of Geophysical Research: Atmospheres, 108, 4783, 10.1029/2003JD003757ï, 2001.

Ashpole, I. and Washington, R.: A new high-resolution central and western Saharan summertime dust source map from automated satellite dust plume tracking, Journal of Geophysical Research Atmospheres, 118, 6981–6995, 10.1002/jgrd.50554, 2013.

Avila, A., Queralt-Mitjans, I., and Alarcón, M.: Mineralogical composition of African dust delivered by red rains over northeastern Spain, Journal of Geophysical Research Atmospheres, 102, 21977–21996, 10.1029/97jd00485, 1997.

Barthazy, E., Henrich, W., and Waldvogel, A.: Size distribution of hydrometeors through the melting layer, Atmospheric Research, 47-48, 193–208, 10.1016/S0169-8095(98)00065-9, 1998.

Bencherif, H., Bounhir, A., Bègue, N., Millet, T., Benkhaldoun, Z., Lamy, K., Portafaix, T., and Gadouali, F.: Aerosol distributions and Sahara dust transport in southern Morocco, from ground-based and satellite observations, Remote Sensing, 14, 10.3390/rs14102454, 2022.

Bish, D. L. and Post, J. E.: Quantitative mineralogical analysis using the Rietveld full-pattern fitting method, American Mineralogist, 78, 10.2138/am-1993-9-1002, 1993.

Bukowiecki, N., Weingartner, E., Gysel, M., Coen, M. C., Zieger, P., Herrmann, E., Steinbacher, M., Ga¨ggeler, H. W., and Baltensperger, U.: A Review of more than 20 years of aerosol observation at the high altituder research station Jungfraujoch, Switzerland (3580 m asl), Aerosol and Air Quality Research, 16, 764–788, 10.4209/aaqr.2015.05.0305, 2016.

Buseck, P. R. and Pósfai, M.: Airborne minerals and related aerosol particles: Effects on climate and the environment, Proceedings of the National Academy of Sciences of the United States of America, 96, 10.1073/pnas.96.7.3372, 1999.

Caquineau, S., Gaudichet, A., Gomes, L., Magonthier, M. C., and Chatenet, B.: Saharan dust: Clay ratio as a relevant tracer to assess the origin of soil-derived aerosols, Geophysical Research Letters, 25, 983–986, 10.1029/98GL00569, 1998.

Cheng, Y.-S., Yeh, H.-C., and Allen, M. D.: Dynamic Shape Factor of a Plate-Like Particle, Aerosol Science and Technology, 8, 109–123, 10.1080/02786828808959176, 1988.

Chester, R. and Johnson, L. R.: Atmospheric dusts collected off the Atlantic coasts of North Africa and the Iberian Peninsula, Marine Geology, 11, 251–260, 10.1016/0025-3227(71)90027-2, 1971.

Chou, C., Stetzer, O., Weingartner, E., Jurányi, Z., Kanji, Z. A., and Lohmann, U.: Ice nuclei properties within a Saharan dust event at the Jungfraujoch in the Swiss Alps, Atmospheric Chemistry and Physics, 11, 4725–4738, 10.5194/acp-11-4725-2011, 2011.

Chou, C., Formenti, P., Maille, M., Ausset, P., Helas, G., Harrison, M., and Osborne, S.: Size distribution, shape, and composition of mineral dust aerosols collected during the African Monsoon Multidisciplinary Analysis Special Observation Period 0: Dust and Biomass-Burning Experiment field campaign in Niger, January 2006, Journal of Geophysical Research: Atmospheres, 113, 10.1029/2008jd009897, 2008.

Coen, M. C., Weingartner, E., Schaub, D., Hueglin, C., Corrigan, C., Henning, S., Schwikowski, M., and Baltensperger, U.: Saharan dust events at the Jungfraujoch: detection by wavelength dependence of the single scattering albedo and first climatology analysis, Atmospheric Chemistry and Physics, 4, 2465–2480, 10.5194/acp-4-2465-2004, 2004.

Collaud Coen, M., Brem, B. T., Gysel-Beer, M., Modini, R., Henne, S., Steinbacher, M., Putero, D., Gini, M. I., and Eleftheriadis, K.: Detection and climatology of Saharan dust frequency and mass at the Jungfraujoch (3580 m asl, Switzerland), EGUsphere preptint, 10.5194/egusphere-2025-4162, 2025.

Cuadros, J., Diaz-Hernandez, J. L., Sanchez-Navas, A., and Garcia-Casco, A.: Role of clay minerals in the formation of atmospheric aggregates of Saharan dust, Atmospheric Environment, 120, 160–172, 10.1016/j.atmosenv.2015.08.077, 2015.

Cuevas-Agulló, E., Barriopedro, D., García, R. D., Alonso-Pérez, S., González-Alemán, J. J., Werner, E., Suárez, D., Bustos, J. J., García-Castrillo, G., García, O., Barreto, Á., and Basart, S.: Sharp increase in Saharan dust intrusions over the western Euro-Mediterranean in February–March 2020–2022 and associated atmospheric circulation, Atmospheric Chemistry and Physics, 24, 4083–4104, 10.5194/acp-24-4083-2024, 2024.

DeCarlo, P. F., Slowik, J. G., Worsnop, D. R., Davidovits, P., and Jimenez, J. L.: Particle morphology and density characterization by combined mobility and aerodynamic diameter measurements. Part 1: Theory, Aerosol Science and Technology, 38, 1185–1205, 10.1080/027868290903907, 2004.

Denjean, C., Cassola, F., Mazzino, A., Triquet, S., Chevaillier, S., Grand, N., Bourrianne, T., Momboisse, G., Sellegri, K., Schwarzenbock, A., Freney, E., Mallet, M., and Formenti, P.: Size distribution and optical properties of mineral dust aerosols transported in the western Mediterranean, Atmospheric Chemistry and Physics, 16, 1081–1104, 10.5194/acp-16-1081-2016, 2016.

Diaz-Hernandez, J. L. and Sanchez-Navas, A.: Saharan dust outbreaks and iberulite episodes, Journal of Geophysical Research, 121, 10.1002/2016JD024913, 2016.

Díaz-Hernández, J. L. and Párraga, J.: The nature and tropospheric formation of iberulites: Pinkish mineral microspherulites, Geochimica et Cosmochimica Acta, 72, 3883–3906, 10.1016/j.gca.2008.05.037, 2008.

Diaz-Hernandez, J. L. and Sanchez-Navas, A.: Saharan dust outbreaks and iberulite episodes, Journal of Geophysical Research: Atmospheres, 121, 7064–7078, 10.1002/2016jd024913, 2016.

Dollase, W. A.: Correction of intensities for preferred orientation in powder diffractometry: application of the March model, Journal of Applied Crystallography, 19, 267–272, 10.1107/s0021889886089458, 1986.

Draxler, R. R. and Rolph, G. D.: HYSPLIT (HYbrid Single-Particle Lagrangian Integrated Trajectory), NOAA Air Resources Laboratory, College Park, MD, 2003.

Dubovik, O., Sinyuk, A., Lapyonok, T., Holben, B. N., Mishchenko, M., Yang, P., Eck, T. F., Volten, H., Muñoz, O., Veihelmann, B., van der Zande, W. J., Leon, J. F., Sorokin, M., and Slutsker, I.: Application of spheroid models to account for aerosol particle nonsphericity in remote sensing of desert dust, Journal of Geophysical Research: Atmospheres, 111, 10.1029/2005jd006619, 2006.

Engelbrecht, J. P. and Derbyshire, E.: Airborne mineral dust, Elements, 6, 10.2113/gselements.6.4.241, 2010.

Feng, J.: A size-resolved model for below-cloud scavenging of aerosols by snowfall, Journal of Geophysical Research Atmospheres, 114, 10.1029/2008JD011012, 2009.

Fiol, L. A., Fornós, J. J., Gelabert, B., and Guijarro, J. A.: Dust rains in Mallorca (Western Mediterranean): Their occurrence and role in some recent geological processes, Catena, 63, 64–84, 10.1016/j.catena.2005.06.012, 2005.

https://doi.org/10.5194/ar-2026-6
Preprint. Discussion started: 4 February 2026

Fischer, A. and Hüglin, C.: Partikelmessungen im NABEL, Messbericht 2024, Empa, Abteilung Luftfremdstoffe/Umwelttechnik, Dübendorf, 2024.

Flentje, H., Briel, B., Beck, C., Collaud Coen, M., Fricke, M., Cyrys, J., Gu, J., Pitz, M., and Thomas, W.: Identification and monitoring of Saharan dust: An inventory representative for south Germany since 1997, Atmospheric Environment, 109, 87–96, 10.1016/j.atmosenv.2015.02.023, 2015.

Francis, D., Fonseca, R., Nelli, N., Bozkurt, D., Picard, G., and Guan, B.: Atmospheric rivers drive exceptional Saharan dust transport towards Europe, Atmospheric Research, 266, 10.1016/j.atmosres.2021.105959, 2022.

Fujiyoshi, Y.: Melting Snowflakes, Journal of the Atmospheric Sciences, 43, 307–311, 10.1175/1520-0469(1986)043<0307:MS>2.0.CO;2, 1986.

Fussell, J. C. and Kelly, F. J.: Mechanisms underlying the health effects of desert sand dust, Environment Intternational, 157, 10.1016/j.envint.2021.106790, 2021.

Grazioli, J., Tuia, D., and Berne, A.: Hydrometeor classification from polarimetric radar measurements: A clustering approach, Atmospheric Measurement Techniques, 8, 149–170, 10.5194/amt-8-149-2015, 2015.

Greenfield, S. M.: Rain scavenging of radioactive particulate matter from
rm the atmosphere, Journal of Meteorology, 14, 115–125, 10.1175/1520-0469(1957)014<0115:Rsorpm>2.0.Co;2, 1957.

Grousset, F. E., Rognon, P., Coudé-Gaussen, G., and Pédemay, P.: Origins of peri-Saharan dust deposits traced by their Nd and Sr isotopic composition, Palaeogeography, Palaeoclimatology, Palaeoecology, 93, 203–212, 10.1016/0031-0182(92)90097-O, 1992.

Haarig, M., Ansmann, A., Engelmann, R., Baars, H., Toledano, C., Torres, B., Althausen, D., Radenz, M., and Wandinger, U.: First triple-wavelength lidar observations of depolarization and extinction-to-backscatter ratios of Saharan dust, Atmospheric Chemistry and Physics, 22, 355–369, 10.5194/acp-22-355-2022, 2022.

Hashino, T., Cheng, K. Y., Chueh, C. C., and Wang, P. K.: Numerical study of motion and stability of falling columnar crystals, Journal of the Atmospheric Sciences, 73, 1923–1942, 10.1175/JAS-D-15-0219.1, 2016.

Herrmann, E., Weingartner, E., Henne, S., Vuilleumier, L., Bukowiecki, N., Steinbacher, M., Conen, F., Collaud Coen, M., Hammer, E., Jurányi, Z., Baltensperger, U., and Gysel, M.: Analysis of long-term aerosol size distribution data from Jungfraujoch with emphasis on free tropospheric conditions, cloud influence, and air mass transport, Journal of Geophysical Research: Atmospheres, 120, 9459–9480, 10.1002/2015jd023660, 2015.

Heymsfield, A. J., Bansemer, A., Poellot, M. R., and Wood, N.: Observations of ice microphysics through the melting layer, Journal of the Atmospheric Sciences, 72, 2902–2928, 10.1175/JAS-D-14-0363.1, 2015.

February 2021: A dusty month for Europe, last

Huang, Y., Kok, J. F., Kandler, K., Lindqvist, H., Nousiainen, T., Sakai, T., Adebiyi, A., and Jokinen, O.: Climate models and remote sensing retrievals neglect substantial desert dust asphericity, Geophysical Research Letters, 47, 10.1029/2019gl086592, 2020.

Hüglin, C., Grange S.K.: Chemical characterisation and source identification of PM10 and PM2.5 in Switzerland, EMPA, Dübendorf, 2021.

Iskandar, F., Chang, H., and Okuyama, K.: Preparation of microencapsulated powders by an aerosol spray method and their optical properties, Advanced Powder Technology, 14, 349–367, 10.1163/15685520360685983, 2003.

Jung, C. H., Um, J., Shin, Y. H., Lee, S. S., Lee, Y. G., Bae, S. Y., and Kim, Y. P.: Minimum collection efficiency diameter during snow scavenging process, Particulate Science and Technology, 33, 321–330, 10.1080/02726351.2014.970311, 2015.

Jurányi, Z., Gysel, M., Weingartner, E., Bukowiecki, N., Kammermann, L., and Baltensperger, U.: A 17 month climatology of the cloud condensation nuclei number concentration at the high alpine site Jungfraujoch, Journal of Geophysical Research, 116, 10.1029/2010jd015199, 2011.

Kajikawa, M.: Observations of the falling motion of plate-like snow crystals part I: The free fall patterns and velocity, Journal of the Meteorological Society of Japan. Ser. II, 70, 1–9, 10.2151/jmsj1965.70.1_1, 1992.

Kandler, K., Schneiders, K., Ebert, M., Hartmann, M., Weinbruch, S., Prass, M., and Pöhlker, C.: Composition and mixing state of atmospheric aerosols determined by electron microscopy: Method development and application to aged Saharan dust deposition in the Caribbean boundary layer, Atmospheric Chemistry and Physics, 18, 13429–13455, 10.5194/acp-18-13429-2018, 2018.

Kandler, K., Benker, N., Bundke, U., Cuevas, E., Ebert, M., Knippertz, P., Rodríguez, S., Schütz, L., and Weinbruch, S.: Chemical composition and complex refractive index of Saharan Mineral Dust at Izaña, Tenerife (Spain) derived by electron microscopy, Atmospheric Environment, 41, 8058–8074, 10.1016/j.atmosenv.2007.06.047, 2007.
Knight, C. A.: Observations of the morphology of melting snow, Journal of Atmospheric Sciences, 1123–1113o, 1979.
Kyrö, E.-M., Grönholm, T., Vuollekoski, H., Virkkula, A., Kulmala, M., Laakso, L., and Kyrö, E.: Snow scavenging of ultrafine particles: field measurements and parameterization, Boreal Environment Research, 14, 11, 10.60910/4x9t-ghuu, 2009.
Laakso, L., Grönholm, T., Rannik, Ü., Kosmale, M., Fiedler, V., Vehkamäki, H., and Kulmala, M.: Ultrafine particle scavenging coefficients calculated from 6 years field measurements, Atmospheric Environment, 37, 3605–3613, 10.1016/S1352-2310(03)00326-1, 2003.
Leinonen, J. and Lerber, A. v.: Snowflake melting simulation using smoothed particle hydrodynamics, Journal of Geophysical Research: Atmospheres, 123, 1811–1825, 10.1002/2017JD027909, 2018.
Ma, C. J., Hwang, K. C., and Kim, K. H.: A novel approach to identifying the elemental composition of individual residue particles retained in single snow crystals, Anal Sci, 29, 849–853, 10.2116/analsci.29.849, 2013.
Magono, C. and Lee, C. W.: Instructions for the use of meteorological classification of natural snow crystals, Journal of the Faculty of Science, Hokkaido University, 7, 1966.
Mallios, S. A., Drakaki, E., and Amiridis, V.: Effects of dust particle sphericity and orientation on their gravitational settling in the earth's atmosphere, Journal of Aerosol Science, 150, 10.1016/j.jaerosci.2020.105634, 2020.
Marticorena, B., Bergametti, G., Aumont, B., Callot, Y., N'Doumé, C., and Legrand, M.: Modeling the atmospheric dust cycle 2. Simulation of Saharan dust sources, Journal of Geophysical Research Atmospheres, 102, 10.1029/96jd02964, 1997.
Martin, S. J., Wang, P. K., and Pruppacher, H. R.: A Theoretical Determination of the Efficiency with which Aerosol Particles are Collected by Simple Ice Crystal Plates, Journal of the Atmospheric Sciences, 37, 1628–1638, 10.1175/1520-0469(1980)037<1628:atdote>2.0.co;2, 1980.
Matsuo, T. and Sasyo, Y.: Melting of snowflakes below freezing level in the atmosphere, Journal of the Meteorological Society of Japan. Ser. II, 59, 10–25, 10.2151/jmsj1965.59.1_10, 1981.
Matzenauer, E.: Tectonics of the Préalpes Klippen and the subalpine molasse (canton Fribourg, Switzerland) doi.org/10.1080/17445647.2025.2509914, 2011.
Mauro, B. D., Garzonio, R., Rossini, M., Filippa, G., Pogliotti, P., Galvagno, M., Cella, U. M. D., Migliavacca, M., Baccolo, G., Clemenza, M., Delmonte, B., Maggi, V., Dumont, M., Tuzet, F., Lafaysse, M., Morin, S., Cremonese, E., and Colombo, R.: Saharan dust events in the European Alps: Role in snowmelt and geochemical characterization, Cryosphere, 13, 1147–1165, 10.5194/tc-13-1147-2019, 2019.
McCorquodale, M. W. and Westbrook, C. D.: TRAIL: A novel approach for studying the aerodynamics of ice particles, Quarterly Journal of the Royal Meteorological Society, 147, 589–604, 10.1002/qj.3935, 2021.
McFarquhar, G. M., Timlin, M. S., Rauber, R. M., Jewett, B. F., Grim, J. A., and Jorgensen, D. P.: Vertical variability of cloud hydrometeors in the stratiform region of mesoscale convective systems and bow echoes, Monthly Weather Review, 135, 3405–3428, 10.1175/MWR3444.1, 2007.
Meier, M. F., Mildenberger, T., Locher, R., Rausch, J., Zünd, T., Neururer, C., Ruckstuhl, A., and Grobéty, B.: A model based two-stage classifier for airborne particles analyzed with Computer Controlled Scanning Electron Microscopy, Journal of Aerosol Science, 123, 1–16, 10.1016/j.jaerosci.2018.05.012, 2018.
Nemuc, A., Vasilescu, J., Talianu, C., Belegante, L., and Nicolae, D.: Assessment of aerosol's mass concentrations from measured linear particle depolarization ratio (vertically resolved) and simulations, Atmospheric Measurement Techniques, 6, 3243–3255, 10.5194/amt-6-3243-2013, 2013.
Nessler, R., Bukowiecki, N., Henning, S., Weingartner, E., Calpini, B., and Baltensperger, U.: Simultaneous dry and ambient measurements of aerosol size distributions at the Jungfraujoch, Tellus B: Chemical and Physical Meteorology, 55, 10.3402/tellusb.v55i3.16371, 2003.
Ohtake, T.: Observations of size distributions of hydrometeors through the melting layer, Journal of the Atmospheric Sciences, 26, 545–557, 10.1175/1520-0469(1969)026<0545:OOSDOH>2.0.CO;2, 1969.
Oraltay, R. and Hallett, J.: The melting layer: A laboratory investigation of ice particle melt and evaporation near 0°C, Applied Meteorology and Climatology, 44, 15, 10.1175/JAM2194.1. , 2005.

https://doi.org/10.5194/ar-2026-6
Preprint. Discussion started: 4 February 2026

Ott, D. K. and Peters, T. M.: A shelter to protect a passive sampler for coarse particulate matter, PM10 − 2.5, Aerosol Science and Technology, 42, 299–309, 10.1080/02786820802054236, 2008.

Panta, A., Kandler, K., Alastuey, A., González-Flórez, C., González-Romero, A., Klose, M., Querol, X., Reche, C., Yus-Díez, J., and Pérez García-Pando, C.: Insights into the single-particle composition, size, mixing state, and aspect ratio of freshly emitted mineral dust from field measurements in the Moroccan Sahara using electron microscopy, Atmospheric Chemistry and Physics, 23, 3861–3885, 10.5194/acp-23-3861-2023, 2023.

Paquet, G., Rognon, P.,Coude-Gaussen G, Wendling R.: Étude minéralogique de poussières sahariennes le long d'un itinéraire entre 19 ° et 35 ° de latitude nord, Revue de géologie dynamique et de géographie physique, 25, 257–265, 1984.

Parajuli, S. P., Jin, Q., and Francis, D.: Editorial: Atmospheric dust: How it affects climate, environment and life on Earth?, Frontiers in Environmental Science, 10, 10.3389/fenvs.2022.1058052, 2022.

Paramonov, M., Virkkula, A., Grönholm, T., Göke, S., and Laakso, L.: Below-cloud scavenging of aerosol particles by snow at an urban site in Finland, Boreal Environment Research 16, 17, 2011.

Párraga, J., Martín-García, J. M., Delgado, G., Molinero-García, A., Cervera-Mata, A., Guerra, I., Fernández-González, M. V., Martín-Rodríguez, F. J., Lyamani, H., Casquero-Vera, J. A., Valenzuela, A., Olmo, F. J., and Delgado, R.: Intrusions of dust and iberulites in Granada basin (Southern Iberian Peninsula). Genesis and formation of atmospheric iberulites, Atmospheric Research, 248, 10.1016/j.atmosres.2020.105260, 2021.

Peng, L. and Liu, Y.: Theoretical foundation of the relationship between three definitions of effective density and particle size, Atmosphere, 13, 10.3390/atmos13040564, 2022.

Pouchou, J. L. and Pichoir, F.: PAP f(ρz) procedure for improved quantitative microanalysis, in: Microbeam Analysis, edited by: Armstrong, J. T., San Francisco Press, 103–106, 1985.

Praz, C., Roulet, Y. A., and Berne, A.: Solid hydrometeor classification and riming degree estimation from pictures collected with a Multi-Angle Snowflake Camera, Atmospheric Measurement Techniques, 10, 1335–1357, 10.5194/amt-10-1335-2017, 2017.

Prodi, F.: Scavenging of Aerosol Particles by Growing Ice Crystals, in: International Conference on Cloud Physics, 1976, 70–75,

Pruppacher, H. R. and Klett, J. D.: Microphysics of Clouds and Precipitation, Springer Netherlands 2010.

Rautela, K. S., Singh, S., and Goyal, M. K.: Characterizing the spatio-temporal distribution, detection, and prediction of aerosol atmospheric rivers on a global scale, J Environ Manage, 351, 119675, 10.1016/j.jenvman.2023.119675, 2024.

Reid, E. A., Reid, J. S., Meier, M. M., Dunlap, M. R., Cliff, S. S., Broumas, A., Perry, K., and Maring, H.: Characterization of African dust transported to Puerto Rico by individual particle and size segregated bulk analysis, Journal of Geophysical Research: Atmospheres, 108, 10.1029/2002jd002935, 2003.

Rolph, G., Stein, A., and Stunder, B.: Real-time Environmental Applications and Display sYstem: READY, Environmental Modelling and Software, 95, 210–228, 10.1016/j.envsoft.2017.06.025, 2017.

Santachiara, G., Prodi, F., Belosi, F., and Nicosia, A.: A Review of Thermo- and Diffusio-Phoresis in the Atmospheric Aerosol Scavenging Process. Part 2: Ice Crystal and Snow Scavenging, Atmospheric and Climate Sciences, 13, 466–477, 10.4236/acs.2023.134026, 2023.

Santos, D., Maurício, A. C., Sencadas, V., Santos, J. D., Fernandes, M. H., and Gomes, P. S.: Spray Drying: An Overview, in: Biomaterials - Physics and Chemistry - New Edition, InTech, 2018.

Scheuvens, D., Schütz, L., Kandler, K., Ebert, M., and Weinbruch, S.: Bulk composition of northern African dust and its source sediments — A compilation, Earth-Science Reviews, 116, 170–194, 10.1016/j.earscirev.2012.08.005, 2013.

Schwikowski, M., Seibert, P., Baltensperger, U., and Gaggeler, H. W.: A study of an outstanding Saharan dust event at the high-alpine site Jungfraujoch, Switzerland, Atmospheric Environment, 29, 1829–1842, 10.1016/1352-2310(95)00060-c, 1995.

Slinn, W. G. N.: Some approximations for the wet and dry removal of particles and gases from the atmosphere, Water, Air, and Soil Pollution, 7, 10.1007/bf00285550, 1977.

Stringham, G. E., Simons, D. B., and Guy, H. P.: The behavior of large particles falling in quiescent liquids2330-7102, 10.3133/pp562C, 1969.

Tagliavini, G., McCorquodale, M., Westbrook, C., Corso, P., Krol, Q., Holzner, M., Tagliavini, G., McCorquodale, M., Westbrook, C., Corso, P., and Krol, Q.: Drag coefficient prediction of complex-shaped snow particles falling in air beyond the Stokes regime., International Journal of Multiphase Flow, 140, 103652, 10.3929/ethz-b-000480012, 2021.

https://doi.org/10.5194/ar-2026-6
Preprint. Discussion started: 4 February 2026

Tobias, A., Karanasiou, A., Amato, F., Roqué, M., and Querol, X.: Health effects of desert dust and sand storms: A systematic review and meta-analysis protocol, 2019.
Trümpy, R.: Geology of Switzerland: An outline of the geology of Switzerland, Wepf & Company 1980.
van der Does, M., Knippertz, P., Zschenderlein, P., Giles Harrison, R., and Stuut, J. W.: The mysterious long-range transport of giant mineral dust particles, Sci Adv, 4, eaau2768, 10.1126/sciadv.aau2768, 2018.
Velasco-Merino, C., Mateos, D., Toledano, C., Prospero, J. M., Molinie, J., Euphrasie-Clotilde, L., González, R., Cachorro, V. E., Calle, A., and de Frutos, A. M.: Impact of long-range transport over the Atlantic Ocean on Saharan dust optical and microphysical properties based on AERONET data, Atmospheric Chemistry and Physics, 18, 9411–9424, 10.5194/acp-18-9411-2018, 2018.
Volken, M. and Schumann, T.: A critical review of below-cloud aerosol scavenging results on Mt. Rigi, Water, Air, & Soil Pollution, 68, 15–28, 10.1007/bf00479390, 1993.
Vollmer, M. K., Steinbacher, M., Leuenberger, M. C., and Emmenegger, L.: The new 2020 air sampling inlet system at Jungfraujoch, International Foundation HFSJG, 2020.
Wang, X., Cao, L., Wu, J., Zhu, G., Zhu, X., Zhang, X., Han, D., Shui, N., Ni, B., and Li, J.: Exploring the Mechanisms of Arsenic Trioxide (Pishuang) in Hepatocellular Carcinoma Based on Network Pharmacology, Evid Based Complement Alternat Med, 2021, 5773802, 10.1155/2021/5773802, 2021.
Weinbruch, S., Wentzel, M., Kluckner, M., Hoffmann, P., and Ortner, H. M.: Characterization of individual atmospheric particles by element mapping in electron probe microanalysis, Mikrochimica Acta, 125, 137–141, 10.1007/bf01246176, 1997.
Weinzierl, B., Sauer, D., Esselborn, M., Petzold, A., Veira, A., Rose, M., Mund, S., Wirth, M., Ansmann, A., Tesche, M., Gross, S., and Freudenthaler, V.: Microphysical and optical properties of dust and tropical biomass burning aerosol layers in the Cape Verde region—an overview of the airborne in situ and lidar measurements during SAMUM-2, Tellus B: Chemical and Physical Meteorology, 63, 10.1111/j.1600-0889.2011.00566.x, 2011.
Weinzierl, B., Ansmann, A., Prospero, J. M., Althausen, D., Benker, N., Chouza, F., Dollner, M., Farrell, D., Fomba, W. K., Freudenthaler, V., Gasteiger, J., Groß, S., Haarig, M., Heinold, B., Kandler, K., Kristensen, T. B., Mayol-Bracero, O. L., Müller, T., Reitebuch, O., Sauer, D., Schäfler, A., Schepanski, K., Spanu, A., Tegen, I., Toledano, C., and Walser, A.: The Saharan aerosol long-range transport and aerosol–cloud-interaction experiment: Overview and selected highlights, Bulletin of the American Meteorological Society, 98, 1427–1451, 10.1175/bams-d-15-00142.1, 2017.
Wiedensohler, A., Birmili, W., Nowak, A., Sonntag, A., Weinhold, K., Merkel, M., Wehner, B., Tuch, T., Pfeifer, S., Fiebig, M., Fjäraa, A. M., Asmi, E., Sellegri, K., Depuy, R., Venzac, H., Villani, P., Laj, P., Aalto, P., Ogren, J. A., Swietlicki, E., Williams, P., Roldin, P., Quincey, P., Hüglin, C., Fierz-Schmidhauser, R., Gysel, M., Weingartner, E., Riccobono, F., Santos, S., Grüning, C., Faloon, K., Beddows, D., Harrison, R., Monahan, C., Jennings, S. G., O'Dowd, C. D., Marinoni, A., Horn, H. G., Keck, L., Jiang, J., Scheckman, J., McMurry, P. H., Deng, Z., Zhao, C. S., Moerman, M., Henzing, B., de Leeuw, G., Löschau, G., and Bastian, S.: Mobility particle size spectrometers: harmonization of technical standards and data structure to facilitate high quality long-term observations of atmospheric particle number size distributions, Atmospheric Measurement Techniques, 5, 657–685, 10.5194/amt-5-657-2012, 2012.
Yan, S. and Palacios, J.: A physics-based sphericity, drag coefficient and Nusselt number model of a partially-melted ice crystal, International Journal of Thermal Sciences, 197, 108798, 10.1016/j.ijthermalsci.2023.108798, 2024.